수리자극에 의한 지열저류층에서의 유도지진과 단층대의 변형에 관한 입자기반 개별요소법 모델링 연구

윤정석*, 아미르 하킴하쉐미, 아노 짱, 귄터 찜머만

Particle Based Discrete Element Modeling of Hydraulic Stimulation of Geothermal Reservoirs, Induced Seismicity and Fault Zone Deformation

Jeoung Seok Yoon*, Amir Hakimhashemi, Arno Zang, Günter Zimmermann

Abstract This numerical study investigates seismicity and fault slip induced by fluid injection in deep geothermal reservoir with pre-existing fractures and fault. Particle Flow Code 2D is used with additionally implemented hydro-mechanical coupled fluid flow algorithm and acoustic emission moment tensor inversion algorithm. The output of the model includes spatio-temporal evolution of induced seismicity (hypocenter locations and magnitudes) and fault deformation (failure and slip) in relation to fluid pressure distribution. The model is applied to a case of fluid injection with constant rates changing in three steps using different fluid characters, i.e. the viscosity, and different injection locations. In fractured reservoir, spatio-temporal distribution of the induced seismicity differs significantly depending on the viscosity of the fracturing fluid. In a fractured reservoir, injection of low viscosity fluid results in larger volume of induced seismicity cloud as the fluid can migrate easily to the reservoir and cause large number and magnitude of induced seismicity in the post-shut-in period. In a faulted reservoir, fault deformation (co-seismic failure and aseismic slip) can occur by a small perturbation of fracturing fluid (<0.1 MPa) can be induced when the injection location is set close to the fault. The presented numerical model technique can practically be used in geothermal industry to predict the induced seismicity pattern and magnitude distribution resulting from hydraulic stimulation of geothermal reservoirs prior to actual injection operation.

Key words Reservoir stimulation, Fluid injection, Induced seismicity, Fault slip, Particle flow code

초 록 본 수치해석논문에서는 절리와 단층대를 포함한 지열저류층에 수리자극을 가할 시 수반되는 유도지진과 단층대의 변형을 개별요소법을 사용하여 모델링하였다. 수채해석기법은 2차원 입자유동코드를 기반으로 하며 수리역학적 상호작용기법과 미소파괴음의 모멘트텐서 역산알고리즘이 결합되었다. 수치해석의 주요결과로는 시공간적으로 변하는 유도지진의 분포와 규모 그리고 단층대의 변형(파괴 및 전단변위)과 주입유체압력의 시공간적 분포와의 상관관계이다. 첫 번째 수치해석으로부터 절리가 분포하는 지열저류층에서의 수리자극에 의한 유도지진의 분포는 주입유체의 점성에 상당한 영향을 받는 것으로 나타났다. 주입유체의 점성이 낮은 경우 (1 cP), 유도지진의 발생범위가 큰 것으로 나타났으며, 주입 후 발생하는 유도지진의 개수와 규모 또한 높게 나타났다. 단층대가 존재하는 지열저류층의 수리자극 모델링의 결과, 주입정의 위치가 단층대와 가까운 경우 작은 주입수 압력분포(<0.1 MPa)로도 단층대의 파괴와 전단변형을 일으킬 수 있는 것으로 나타났다. 본 논문에서 소개한 수치해석기법은 수리자극을 통한 지열저류층 개발 시 유도지진의 분포와 규모를 실제 유체주입작업 전에 예측할 수 있게 함으로써 지열에너지개발 분야에서 유용하게 사용될 수 있을 것으로 기대한다.

핵심어 저류층 수리자극, 유체주입, 유도지진, 단층전단, 입자유동코드

*Corresponding Author: Jeoung Seok Yoon
Tel) +493312881716, Fax) +493312881127
E-Mail) jsyoon@gfz-potsdam.de
Helmholtz-Zentrum Potsdam, Deutsches GeoForschungs-Zentrum GFZ, Telegrafenberg 14473, Potsdam, Germany

1. INTRODUCTION

Developing an Enhanced Geothermal System (EGS) in deep reservoir requires creation of highly permeable heat exchanger which is usually achieved by performing hydraulic fracturing. Fluid injection can cause stress field changes, re-activation of pre-existing joints and slip of nearby faults which can consequently trigger larger magnitude events, e.g. local magnitude of 3.4 event in Basel EGS operation (Kraft et al. 2009). These largest events tend to occur on the fringes, outside the "main cloud" of seismicity and are often observed after well shut-in, making them difficult to control (Mukuhira et al. 2013). Therefore, the need for understanding of the processes underlying the occurrence of induced seismicity, in particular, post-shut-in seismicity has become an important issue worldwide (Majer et al. 2007). Such phenomena have led to development of numerical tools that are able to simulate fluid injection in rock mass and interactions between injected fluid, rock mass and joints, creation of new fractures and re-activation of pre-existing joints and faults.

So far, several studies have been carried out in order to understand the coupling between the spatio-temporal stress changes and the seismicity in the geothermal reservoirs and their vicinities (Hakimhashemi et al. 2013). The corresponding geomechanical models contain different processes such as pore pressure diffusion (Kohl and Mégel 2007, McClure and Horne 2011), the pore pressure stress coupling process (Altmann et al. 2010, Hillis 2000), thermal diffusion and combination of these processes (Baisch et al. 2010, Bruel 2007, Rutqvist et al. 2007, Schoenball et al. 2010). The outputs of these models are in form of spatio-temporal stress changes in the reservoir.

Induced seismicity can be simulated from the stress changes (obtained from geomechanical model) only by considering additional processes and assumptions on the parameters corresponding to the failure processes (Bruel 2007). The actual rupture process has already been simulated for 2D reservoir models (Yoon et al. 2013, Zang et al. 2013).

Appropriate measure for mitigation of large magnitude events and optimization of heat exchanger can be established after reliability of the numerical tools is validated.

In this context, the current study is a step forward of the 2D reservoir model of Yoon et al. (2013) and Zang et al. (2013) applied to simulation of induced seismicity and triggered fault slip by hydraulic stimulation of a synthetic reservoir. Hydraulic stimulation is tested on two different synthetic reservoirs subjected to differential in-situ stresses.

Main interest is to examine how the synthetic reservoirs behave under different viscosity of fracturing fluid. Another model is aimed at examining the influence of injection location on the behavior of major fault that is cutting across the reservoir and initially at critically stressed state.

Section 2 briefly introduces the modeling method. Section 3 and 4 present modeling procedure and results, respectively, which are then followed by discussion and a few conclusions.

2. METHODOLOGY

2.1 Particle Flow Code 2D (PFC2D)

PFC2D is a two-dimensional distinct element geomechanical modeling software (Itasca 2008). The material simulated, in this case a reservoir rock mass, is modeled as an aggregate of circular particles bonded at their contacting points with finite thickness of cementing around the contact (referred to hereafter as Bonded Particle Model, BPM). Under an applied load, the bonds can break in Mode I (tensile crack) or Mode II (shear crack). In BPM, there are several assumptions: 1) particles are rigid and circular with finite mass, 2) particles move independently and can both translate and rotate, 3) particles interact only at contacts allowing some overlap, i.e. soft contact. The calculation cycle in PFC2D is a time stepping algorithm that requires repeated application of the law of motion applied to each particle and a linear force displacement law applied to each contact. For more detail, we refer to Potyondy and Cundall (2004).

2.2 Fluid flow algorithm

Flow of viscous fluid in BPM and fluid volume and pressure driven breakages of bonds in Mode I and
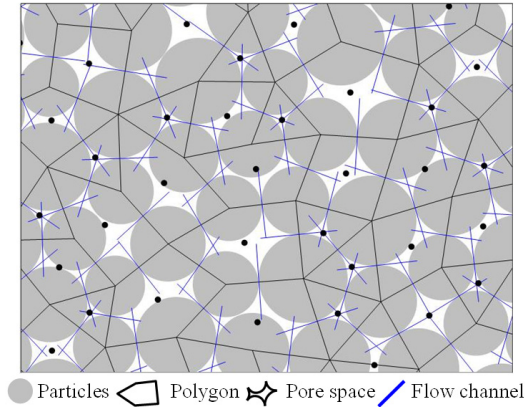
Fig. 1. Pore network model. Flow channels (blue lines at the particle contacts) are connecting two neighboring pore spaces bounded by polygons. Black dots at the polygon centers are virtual pores where pressure is stored

Mode II are simulated in Hazzard et al. (2002) and Zang et al. (2013). Fluid flow is simulated by assuming that each bonded contact is a flow channel (Fig. 1, blue lines) and these channels connect up pore spaces (Fig. 1, white spaces in each closed polygon) where fluid pressure can be stored. Fluid flow is driven by the pressure difference between two neighboring pore spaces and governed by Cubic law (equation 1) assuming that the flow is laminar between the two smooth parallel plates:

$$q = (e^3 \Delta P_f)/(12\eta L) \qquad (1)$$

where, e is hydraulic aperture, ΔP_f is fluid pressure difference between two neighboring pores, L is flow channel length (= average diameter of two neighboring particles), η is fluid dynamic viscosity.

Hydraulic aperture e, of the flow channel changes as a function of normal stress σ_h, using the equation (Hökmark et al. 2010, Zang et al. 2013):

$$e = e_{inf}+(e_0-e_{inf})\exp(-0.15\sigma_h) \qquad (2)$$

where, e_{inf} is hydraulic aperture at infinite normal stress (= 50 microns), e_0 is hydraulic aperture at zero normal stress (= 650 microns), σ_h is effective normal stress. The e_0 is back-calculated from an assumed permeability of the synthetic reservoir, k (= 10^{-12} m^2)

(Hazzard et al. 2002, Zang et al. 2013).

Fluid pressure increases per time step in a pore space is computed using equation (3) which is a function of fluid bulk modulus K_f, volume of pore space V_d, sum of flow volume (entering and leaving the pore space) and volume change of pore space ΔV_d, due to mechanical loading.

$$\Delta P_f = K_f(\Sigma q \Delta t - \Delta V_d)/V_d \qquad (3)$$

The force term that is applied to the particles surrounding a pore space is a product of fluid pressure and the particle surface on which the fluid pressure exerts. The force moves the particles which consequently changes the stress states at the surrounding particle contacts, which in turn changes the hydraulic aperture and thereby flow field.

2.3 Seismicity computation

Each bond breakage in BPM is assumed to be a fracture process associated with radiation of seismic energy. The simulation runs in dynamic mode with realistic level of energy attenuation in rock using seismic quality factor Q which is then converted to a local damping coefficient ($a = \pi/2Q$) assigned to the particles. Upon a bond breakage, part of accumulated strain energy at the broken bond is released to the surrounding in a form of seismic wave. A numerical technique for calculating the seismic source information, e.g. moment tensor components (M_{ij}), seismic moment (M_0), moment magnitude (M_w), source mechanism, in PFC2D and 3D has been proposed by Hazzard and Young (2002, 2004) and used in a number of numerical studies (Hazzard et al. 2002, Al-Busaidi et al. 2005, Zhao and Young 2011, Yoon et al. 2012, 2013, Zang et al. 2013).

Seismicity computation algorithm starts with an assumption that each bond breakage represents a single crack. When a bond breaks, the two particles on either side of the crack (called 'source particle') move and contacts surrounding the source particles suffer some deformation. Therefore, there will be a force change at the surrounding contact due to the formation of the cracks. Moment tensor (2x2 as this study used PFC2D) is built by integrating the moments (product
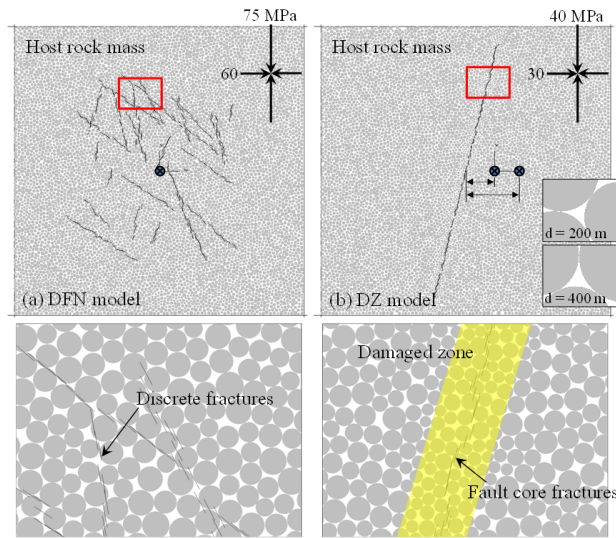
Fig. 2. (a) DFN model with embedded discrete fractures with arbitrary length and orientation and (b) DZ model with through-going deformation zone represented by damaged zone and fault core fractures. Both models are subjected to differential in-situ stresses. Bottom two figures are enlarged view of the box area. For the DZ model, particle arrangement surrounding the void spaces serving as injection points at 200 and 400 m distance from the fault is depicted in two inset figures

of force change and distance between the contact point and the event centroid) at the contacts surrounding the crack. The moment tensor built in this way evolves with time, i.e. full time-dependent quantity. However, in PFC2D, only a single moment tensor is stored for each event where the scalar seismic moment M_0 records the maximum value (Hazzard and Young 2002, 2004). This approach calculates the seismic moment of the induced event only at the instance of bond breakage. However, those smooth joints that are initially unbonded (failed after in-situ stresses are applied) undergo frictional slip. The moment tensor approach is not able to capture the seismic source information of such aseismic slip event.

3. MODELING PROCEDURE

The reservoir model is 2 x 2 km in size. Diameters of the particles to pack the given space are in range between 20-30 m. The diameter range chosen is comparable to that used in a similar study by Hazzard et al. (2002) where they modeled fluid injection and induced seismicity in synthetic but targeted on Soultz geothermal reservoir, using average particle diameter

= 19.7 m and the Block-Spring model by Baisch et al. (2010) where they also simulated fluid injection induced seismicity at Soultz, with fracture zone consisting of individual blocks, i.e. slip patches, of 20 m side length.

Fluid injection simulation is done on two different models; one with scattered discrete joints with arbitrary length and orientations (Fig. 2a, referred to hereafter DFN (Discrete Fracture Network) model) and the other with through-going deformation zone in relatively intact host rock mass (Fig. 2b, referred to hereafter DZ (Deformation Zone) model). Deformation zone is represented by collection of particles with smaller radii compared to surrounding particles representing host rock mass. The bond strength of the particles in the deformation zone is assigned with lower tensile and cohesion strength compared to the host rock mass. Within the deformation zone, smooth joint bonds are used to represent fault core fractures that can slip with certain level of dilation.

For DFN model, injection is applied at the model centre with changing rate in three steps (Fig. 3, 10, 12.5, 15 l/s maintained for 2 hours each). Viscosity of the injection fluid has two variations: 1 cP and 500
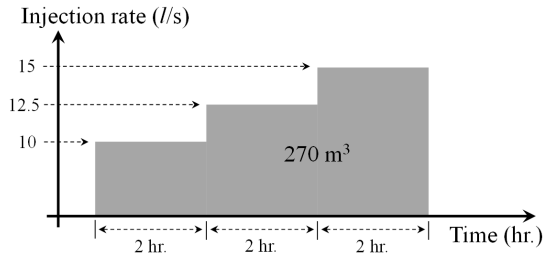
Injection rate (*l*/s)

Fig. 3. Applied injection rate for hydraulic stimulation simulations of DFN models and DZ models

cP. For DZ model, injection is applied at 200 and 400 m away from the deformation zone with constant rate changing also in three steps (Fig. 3). The total volume of fluid injected is, therefore, 270 m³. For the DZ model, particle arrangement surrounding the void spaces serving as injection points at 200 and 400 m distance from the fault is depicted in two inset figures.

In-situ stresses are different in two models. DFN model is subjected to far-field major and minor principal stresses with 75 MPa (in North-South) and 60 MPa (in West-East). This in-situ stress set is taken from Cornet et al. (2007, eqn.1b and 1c) assuming that the 2D section is located at 4 km depth. For the DZ model, 40 and 30 MPa are applied in N-S and W-E directions, respectively. This stress set is also taken from Cornet et al. (2007, eqn 1b and 1c) assuming that the reservoir section is located at relatively shallow depth, 2.2-2.3 km. Along and near the boundaries, 150 m thick region is assigned with high viscous

Table 1. Mechanical properties of the model components

	Properties	Unit	DFN model	DZ model
Host rock mass (enhanced parallel bond model)	Particle density	kg/m³	2600	2630
	Friction coefficient	-	0.9	0.9
	Young's modulus	GPa	60	50
	Poisson's ratio	-	0.25	0.25
	Tensile strength, mean±std.dev.	MPa	11.5±1.5	9±6
	Cohesion, mean±std.dev.	MPa	30±5	25±7
	Friction angle	Degree	52	53
Damaged zone (enhanced parallel bond model)	Particle density	kg/m³		2630
	Friction coefficient	-		0.9
	Young's modulus	GPa		30
	Poisson's ratio	-	NA	0.25
	Tensile strength, mean±std.dev.	MPa		2±0.5
	Cohesion, mean±std.dev.	MPa		5±1
	Friction angle	Degree		30
Discrete joints in the DFZ model & Fault core fractures in the DZ model (smooth joint bond model)	Normal stiffness	GPa/m	200	300
	Shear stiffness	GPa/m	50	50
	Friction coefficient	-	0.9	0.9
	Tensile Strength	MPa	0	1
	Cohesion	MPa	0.5	5
	Friction angle	Degree	30	30
	Dilation angle	Degree	3	3

Table 2. Modeling scenario and parameter variations

Parameters	DFN model	DZ model
Injection fluid viscosity	1 cP vs. 500 cP	1 cP
Injection point location	At model centre	200 m vs. 400 m*
In-situ stresses (SH & Sh)**	75 MPa (N-S), 60 MPa (W-E)	40 MPa (N-S), 30 MPa (W-E)

* Distance *d* from the deformation zone
** SH and Sh are calculated from eqn. 1b and 1c of Cornet et al. (2007).

damping properties to minimize wave reflection. In total, results of four model runs are presented. Table 1 lists the mechanical properties of the model components and Table 2 summarizes modeling scenarios and key variations in the model parameters.

4. MODELING RESULTS

4.1 DFN model: Effect of fluid viscosity

Fig. 4 shows results of DFN models subjected to different injection fluid viscosity: (a) 1 cP, (b) 500 cP. Top left ordinate is the applied rate of injection. Right ordinate is the fluid pressure monitored at the injection point (fluid pressure P_f at the pore space where injection is applied). Bottom left ordinate is

moment magnitude (M_w) of the induced seismic events and right ordinate shows radiated seismic energy (E_s) of the induced events calculated from the moment magnitude M_w using the equation below (Gutenberg and Richter 1956):

$$\log_{10}(E_s) = 4.8 + 1.5 M_w \tag{4}$$

Comparing with a few field observations, a few similarities can be found: (1) instantaneous increase of the P_f with flow rate increase, (2) instantaneous drop of fluid pressure with occurrence of induced events, (3) decreasing fluid pressure at the onset of shut-in, (4) lower seismicity rate in the post-shut-in period, and (5) large magnitude events in the post-
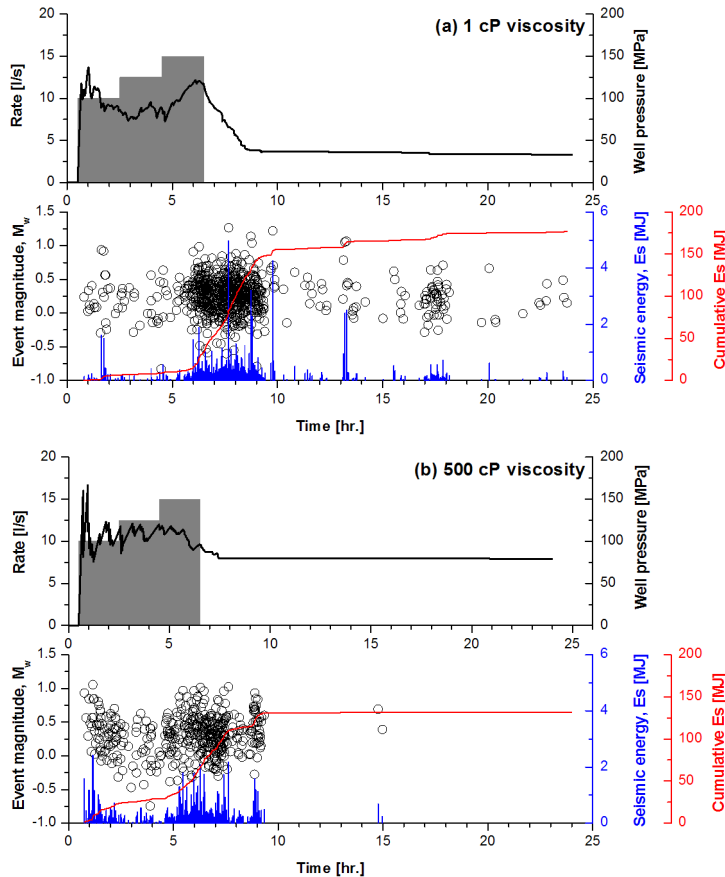

Fig. 4. Results of hydraulic stimulation simulation using (a) 1 cP and (b) 500 cP viscosity fracturing fluid in DFN model (top left: applied rate of injection at model centre, top right: simulated fluid pressure at the injection point pore space, bottom left: moment magnitude M_w of the induced seismic events, bottom right: radiated seismic energy E_s of the induced seismic events)
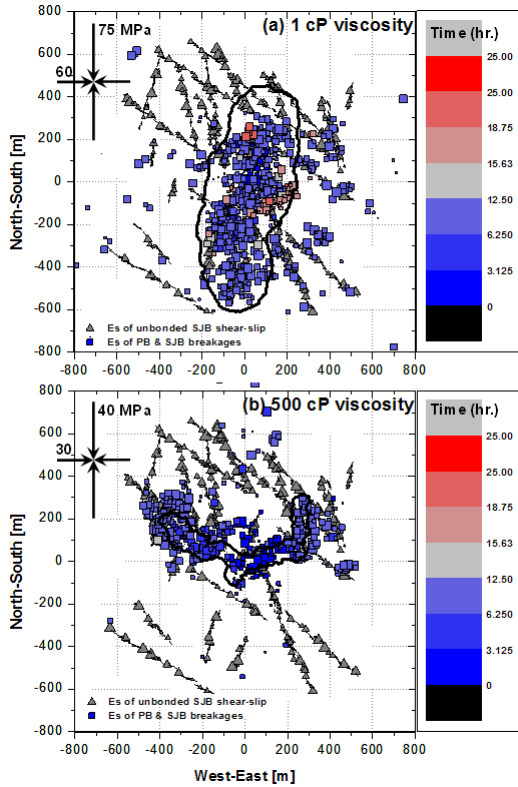
Fig. 5. Spatio-temporal distributions of the induced seismic events in DFN models subjected to fluid injection with (a) 1 cP and (b) 500 cP viscosity. Occurrence time of the events (only for the dotted symbols) is depicted by the color scale. Triangle symbol represents the frictional slip events at the unbonded smooth joints. Symbol size is proportional to the seismic radiated energy *Es*. Black contour depicts the spatial distribution of 0.1 MPa fluid pressure at 25 hours

shut-in period.

Fig. 5a shows the spatio-temporal distribution of the induced seismic events for the case of the injection fluid with viscosity of 1 cP. Color scale depicts the occurrence time of the induced events. Size of the symbol is proportional to the radiated seismic energy, *E*s. Dotted symbols are those seismic events computed by the moment tensor method (Hazzard and Young 2002, 2004) where seismic source information data, e.g. seismic moment (M_0), moment magnitude (M_w), and source mechanisms, are computed only at the instance of bond breakages (Mode I and Mode II). Triangle symbols are those seismic events occurring at the

unbonded smooth joints by frictional sliding. Seismic moment M_0 of such slipping event is computed as a function of shear modulus G (30 GPa), rupture surface area A (m^2) and shear slip displacement $\underline{d}$ (m) (equation 5 from Kramer (1996)). It is then converted to moment magnitude by using equation 6 from Hank and Kanamori (1979).

$$M_0 = GA\underline{d} \tag{5}$$

$$M_w = (2/3)\log_{10}(M_0)+6 \tag{6}$$

Black contour in Fig. 5a presents spatial distribution of 0.1 MPa fluid pressure. Inner and outer regions of the contour represent the areas where the fluid pressure is larger and less than 0.1 MPa, respectively. This 0.1 MPa fluid pressure contour is chosen to visualize the fluid migration front.

Fracture initiates near the injection point and propagates mostly downward and turn its direction from S-W to S-E (Fig. 5a). Most of the events are confined within the fluid pressure distribution contour indicating that the major driving force for the event occurrence is the increased fluid pressure. However, a few events occurred outside of the fluid pressure contour. These events are mostly at the pre-existing joints and indicate that the re-activation of the pre-existing joints can occur by small perturbation (< 0.1 MPa) of the fluid pressure. There are relatively large number of events occurred after shut-in (during 6.5-10 hr.). This is where the well pressure is dropping rapidly. Fig. 6 shows the 0.1 MPa fluid pressure contours evolving with time after well shut-in (t = 6.5 hr.) in (a) 1 cP case and (b) 500 cP case. The figures clearly show significant difference in speed and extent of fluid migration after well shut-in. The time range from 6 to 9.5 hours is where the P_f at the time of shut-in (120 MPa) decreased rapidly to 50 MPa. Such rapid relaxation caused shock in the reservoir and resulted in many events at the pre-existing joints that are even far away from the injection point. The results agree with the field observations made by Mukuhira et al. (2013) on Basel EGS induced seismicity cloud. They observed that the large events during the stimulation and just
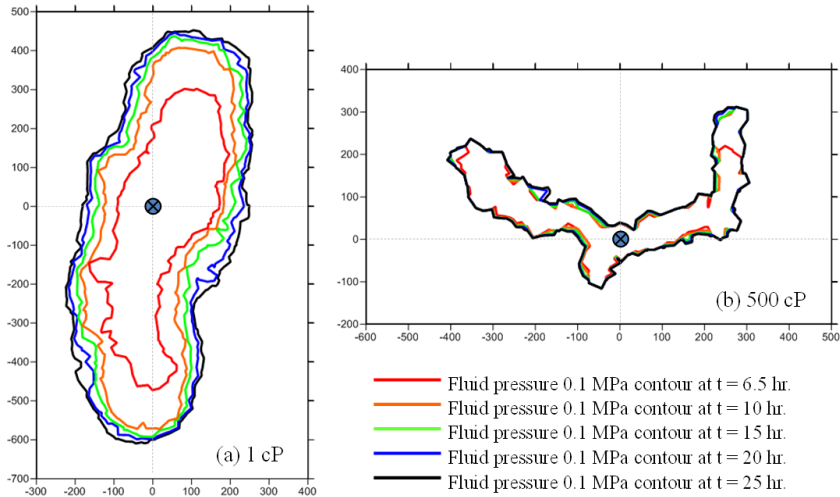
Fig. 6. Contour plots of fluid pressure 0.1 MPa at different time after shut-in (red: at the time of shut-in, 6.5 hr.; orange: at 10 hr.; green: at 15 hr.; blue: at 20 hr.; black: 25 hr.) for injection of (a) 1 cP fracturing fluid and (b) 500 cP fracturing fluid

after bleeding off had hypocenters within the seismic event cloud while the large events that occurred long after shut-in were located outside of the seismic event cloud. Further occurrence of induced events after 10 hours is due to migration of the pressurized fluid. As fluid has low viscosity, fluid can travel and further to surrounding even with low fluid pressure.

When viscosity of injection fluid is changed to 500 cP, the well pressure also decreases at the time of shut-in (Fig. 4b). However, the amount of pressure drop is very small compared to that shown in Fig. 4a. The shape of induced event cloud also differs significantly. In the beginning, the event cloud develops in minimum horizontal stress direction (in W-E), but later changes to maximum horizontal direction (in N-S). Also, the total number of post-shut-in events is less compared to 1 cP viscosity fluid injection. This is due to the high fluid viscosity where additional high pressure is required to push the fluid to move further (Fig. 6b). This result indicates that the viscosity of fracturing fluid has a large impact on the induced seismicity and consequently plays a significant role in optimization of hydraulic stimulation design. The inner area of the 0.1 MPa fluid pressure contour in case of 1 cP viscosity of injection fluid (Fig. 5a) is significantly larger than that of 500 cP case (Fig. 5b).
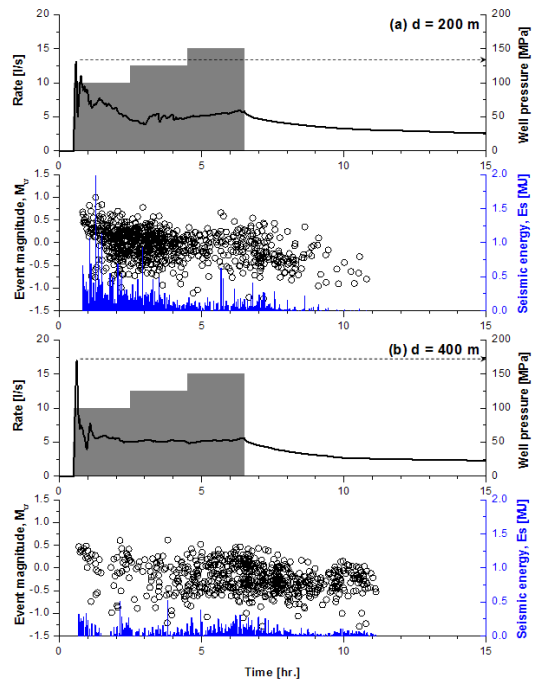

Fig. 7. Results of hydraulic stimulation simulation of DZ model with fluid injection at (a) 200 m and (b) 400 m distance from the deformation zone (top left: applied rate of injection at model centre, top right: simulated fluid pressure at the injection point, bottom left: moment magnitude M_w of the induced seismic events, bottom right: radiated seismic energy Es of the induced seismic events)

4.2 DZ model: Effect of injection with distance from fault

Fig. 7 shows results of DZ models subjected to injection at different locations: (a) 200 m and (b) 400 m distance from the deformation zone. The top left ordinate is applied rate of injection. Right ordinate is the fluid pressure monitored at the injection point. Bottom left ordinate is moment magnitude (M_w) of the induced seismic events and right ordinate shows radiated seismic energy (E_s) of the induced events.

Fig. 8 shows the spatio-temporal distribution of the induced seismicity for both cases (a) d = 200 m and (b) d = 400 m. Similar to the Fig. 5, the color scale depicts the occurrence time of the induced events. Again the size of the symbol is proportional to the radiated seismic energy E_s. Dotted symbols are the seismic events computed by the moment tensor method and triangle symbols are those seismic events occurring at the unbounded smooth joints by frictional sliding.

At the beginning of injection, the well pressure increases rapidly to about < 150 MPa. However, when compared with Fig. 7b, the well pressure peak is less in case (a), where d = 200 m. This is due to large number of triggered events in the deformation zone, i.e. parallel bond breakages in the damaged zone and slipping of unbonded smooth joints of fault core fractures. Such behavior is documented by red events (occurrence time interval: 0.5-2.5 hr.) and orange events (occurrence time interval: 2.5-4.5 hr.) that are concentrated near the injection point as well as along the fault (Fig. 8a). Such events and fault slip resulted in stress drop and displacements of particles. Therefore the initial is-stress state may have changed, which consequently makes the fracture breakdown pressure change (FBP, equation 7 from Zang and Stephansson (2010)).

$$\text{FBP} = (3S_h - S_H + \sigma_t) \qquad (7)$$

where, S_h and S_H are minimum and maximum horizontal in-situ stresses, and σ_t is rock tensile strength. According to FBP equation, and the in-situ stress setting and tensile strength, FBP is calculated to be about 60 MPa (FBP = 3x30-40+9±6 = 53~65 MPa),
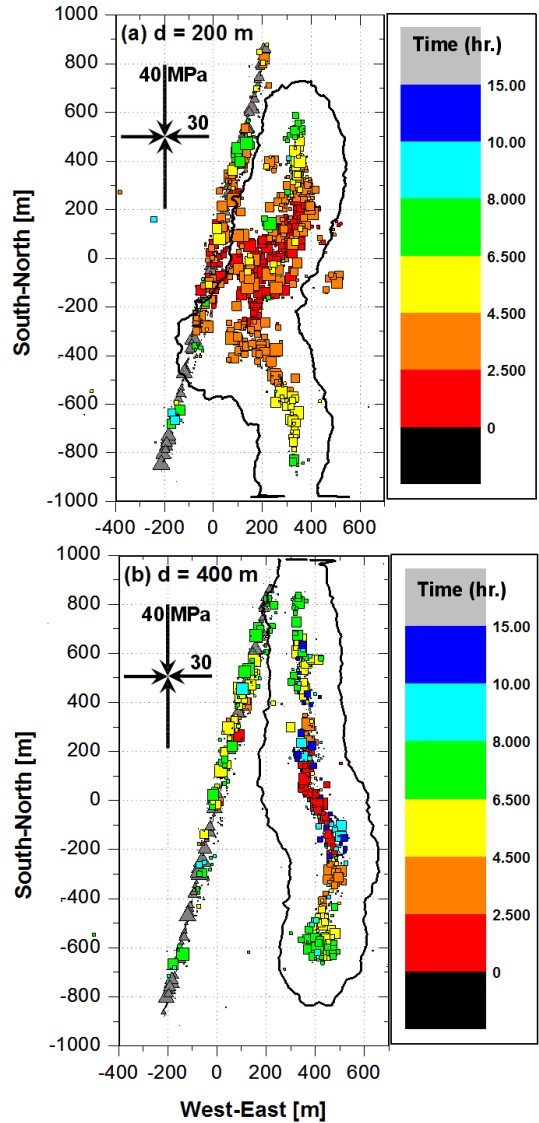

Fig. 8. Spatial and temporal distributions of the induced seismic events in DZ models with fluid injection at (a) 200 m and (b) 400 m distance from the deformation zone. Coordinates of injection points are (200,0) and (400,0) for (a) and (b), respectively. Occurrence time of the events (only for the dotted symbols) is depicted by the color scale. Triangle symbol represents the frictional slip events at the unbounded smooth joints. Symbol size is proportional to the seismic radiated energy E_s. Black contour depicts the spatial distribution of 0.1 MPa fluid pressure at 15 hours

which is far lower than the simulated FBP in both cases (150 MPa). The reason for such big gap is that

the FBP estimated is for a radial tensile fracture developing at the bore hole wall propagating bilaterally along the azimuths 0° and 180°, which are parallel to the S_H direction of the pre-existing virgin far-field stress (Zang and Stephannson 2010). However, in the reservoir model, bore hole geometry is not modeled and the fluid is injected into a void space surrounded by three particles (insets in Fig. 2b). As the fluid migration path is pre-defined by the particle arrangement, e.g. three flow channels (potential fractures), to generate a fracture the fluid pressure should exceed the bond tensile strength plus additional amount that should be given to induce fracture of which planes are not oriented parallel to S_H direction.

Moment magnitudes of the induced events in the early stage of injection (0.5-2.5 hr.) are relatively higher than those shown in Fig. 7b. The maximum value of radiated seismic energy E_s is 2 MJ which is significantly higher than those shown in Fig. 7b (< 0.5 MJ). However, it should be noted that the induced events due to fluid injection and those along the fault are not distinguished in Fig. 7. Further effort on visualization should be made to distinguish them: induced within the fluid migration front vs. induced along the fault and outside of the fluid migration front.

When the location of injection is set further away from the deformation zone, fluid injection has less influence on fault slip. This is documented by red colored events that are mostly concentrated near the injection point but hardly visible along the fault (Fig. 7b).

5. DISCUSSION

In this study, we computed the seismic moment and moment magnitude of the smooth joints that are initially at unbonded state (failed either in Mode I or in Mode II during in-situ stressing of the reservoir with differential stress field) and undergo slip using equation (5). The shear displacement d of the smooth joints are time-dependent quantity. Therefore, the seismic moment of such slip events should change with time depending on the amount of slip displacement changing per time step. In the current study, we only considered the slip displacement of the smooth joints at the final state (23 hr. for DFN model, 15 hr. for DZ model) and computed the corresponding seismic moment and moment magnitude using the equations (5) and (6). These slip events at the pre-existing fractures in DFN model and fault core fractures in DZ model are represented by gray triangle symbols with their size proportional to the radiated seismic energy
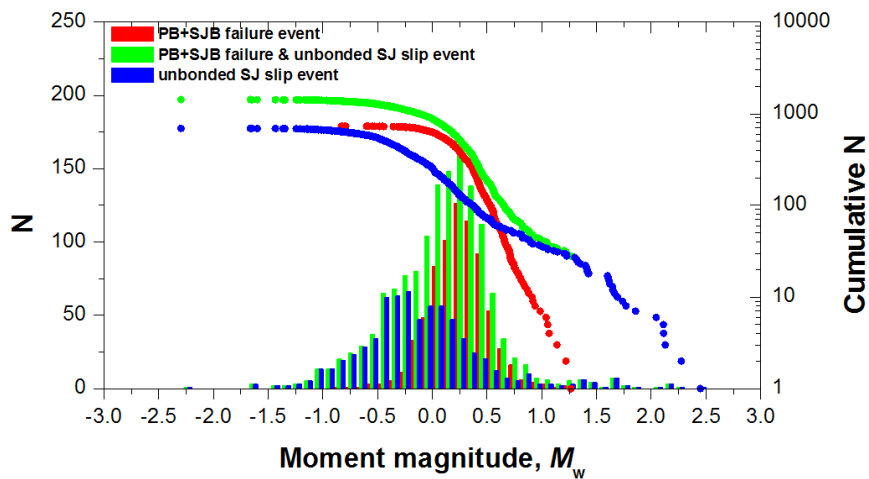

Fig. 9. Histogram of the moment magnitudes M_w of the induced seismic events (left) and the cumulative frequency and magnitude distribution (right) of the induced seismic events computed from bond breakages (red) and bond breakages + shear slip (green) simulated in DFN model with 1 cP viscosity fluid injection. For reference, blue histogram is provided which is frequencymagnitude distribution of the slip events of the unbounded smooth joints

*E*s in unit of kilo Joule.

Fig. 9 shows three histograms of the moment magnitudes of the induced events in DFN model with 1 cP viscosity fluid injection. Red bars correspond to moment magnitudes of the events computed from breakages of parallel bonds and smooth joint bonds using the moment tensor approach (Hazzard and Young 2002, 2004; Zang et al. 2013). Green histogram is where the moment magnitudes data of the unbonded smooth joints by shear slip is added to the red histogram. In general, the frequencies corresponding to the green histogram increases for all given magnitude classes comparing with the frequencies of the red histogram. However, one can clearly see that the left part, i.e. smaller magnitudes range, shows significant increase in its population, which is documented by the blue histogram. This indicates that considering the event magnitudes only from the bond breakages can neglect the significant portion of low magnitude events by shear slip of the joints. Cumulative frequencies of the red and the green histograms are plotted on right ordinate. This is typical way of plotting frequency-magnitude distribution in order to compute the Gutenberg-Richter *b*-values which are very often used in seismology and probabilistic seismic hazard assessment (PSHA) to estimate hazard potential (Hakimhashemi et al. 2013). GutenbergRichter *b*-value is computed as a slope of the linear part of the cumulative frequency and magnitude distribution. Often, least square method (LSM) is used to do linear fitting. However, as selection of linear interval can be subjective, we used in this study maximum likelihood method (MLM) to calculate the *b*-value. The *b*-values calculated for the red distribution is 2.15 (with 95% confidence interval of [1.93, 2.34]), whereas it is 1.52 (with 95% confidence interval of [1.40, 1.64]) for the green distribution. This indicates that, according to frequency-distribution relation, if *b*-value decreases and the number of events simultaneously increases (case green versus case red in Fig. 8), then the occurrence rate of the relatively larger magnitude events also increases. The latter results in seismic hazard increase. This result emphasizes the necessity of developing a seismicity computation algorithm for computing time-dependent aseismic slip of pre-existing joints.

6. CONCLUSIONS

This numerical study investigated hydraulic stimulation in synthetic reservoirs with pre-existing joints and fault using PFC2D with fluid flow and seismicity computation algorithms. Applied rate of injection increases in three steps. Moment magnitudes and seismic radiated energy of the induced seismic events by Mode I and Mode II rock failures and by shear slip that are changing spatially and temporally are investigated with relation to fluid pressure distribution in two different synthetic reservoirs under differential in-situ stresses.

Conclusions are drawn as follows.

1. Discrete fracture network model stimulated by low viscosity fluid injection exhibited elliptical shape of induced event cloud with longer axis parallel to maximum horizontal stress orientation. Injection pressure drops rapidly after shut-in and migration of pressurized fluid continues further into the reservoir and caused additional post-shut-in events until long after the well shut-in.

2. Discrete fracture network model stimulated with 500 cP viscosity fracture fluid exhibited event cloud developed in minimum horizontal stress orientation in early stage of injection, but later turns towards maximum horizontal stress orientation. Injection pressure drops little after shut-in and migration of pressurized fluid is very slow due to high viscosity, which consequently resulted in less post-shut-in events.

3. Deformation zone model stimulated by fluid injection near the fault shows large number of induced and triggered events and fault slip. When the distance between fluid injection and fault increases, triggered events and fault slip of deformation zone are less influenced by the fluid injection. This result indicates that when hydraulic stimulation is operated near a fault that is under critically stressed state, location of fluid injection point should be carefully chosen to avoid slip of fault that can trigger large magnitude events. If the location of fluid injection cannot be changed, one should consider changing the injection strategy, e.g. so-called 'soft

stimulation' as proposed by Zang et al. (2013).

4. Gutenberg-Richter b-values are calculated for the DFN model stimulated by 1 cP viscosity fracturing fluid using maximum likelihood method. Results show that b-value decreases to 1.52 when the moment magnitudes of aseismic shear slip of the joints are taken into account, whereas it is 2.15 without taking into account of those aseismic slip events. This indicates that, from seismological and probability seismic hazard assessment point of view, by neglecting the magnitudes of aseismic slip, the potential induced seismic hazard can be significantly under-estimated. This result emphasizes the necessity of developing a seismicity computation algorithm for computing time-dependent aseismic slip of pre-existing joints.

ACKNOWLEDGEMENT

REFERENCES

1. Altmann J., Müller T., Müller B., Tingay M., Heidbach O. 2010. Poroelastic contribution to the reservoir stress path. International Journal of Rock Mechanics and Mining Sciences 47(7), 1104-1113.

2. Al-Busaidi A., Hazzard J.F., Young R.P. 2005. Distinct element modeling of hydraulically fractured Lac du Bonnet granite. Journal of Geophysical Research 110, B06302, DOI: 10.1029/2004JB003297.

3. Baisch S., Vörös R., Rothert E., Stang H., Jung R., Schellschmidt R. 2010. A numerical model for fluid injection induced seismicity at Soultz-sous-Forêts. International Journal of Rock Mechanics Mining Sciences 47, 405-413.

4. Bruel D. 2007. Using the migration of induced seismicity as a constraint for fractured hot dry rock reservoir modelling. International Journal of Rock Mechanics and Mining Sciences 44, 1106-1117.

5. Cornet F.H., Bérard Th., Bourouis S. 2007. How close to failure is a granite rock mass at a 5 km depth? International Journal of Rock Mechanics Mining Sciences 44, 47-66.

6. Gutenberg B., Richter C.F. 1956. Earthquake magnitude, intensity, energy and acceleration (second paper). Bulletin of the Seismological Society of America 46, 105-145.

7. Hakimhashemi A., Yoon J.S., Heidbach O., Zang A., Grünthal G. 2013. Forward induced seismic hazard assessment (FISHA) application to synthetic seismicity catalog generated by hydromechanical modeling of fluid injection. In: Proceedings of Thirty-Eighth Workshop on Geothermal Reservoir Engineering, Stanford University, Stanford, California, Feb. 11-13, 2013, SGP-TR-198.

8. Hanks T.C., Kanamori H. 1979. A Moment Magnitude Scale. Journal of Geophysical Research 84, 2348-2350.

9. Hazzard J.F., Young R.P. 2002. Moment tensors and micromechanical models. Tectonophysics 356, 181-197.

10. Hazzard J.F., Young R.P. 2004. Dynamic modeling of induced seismicity. International Journal of Rock Mechanics Mining Sciences 41, 1365-1376.

11. Hazzard J.F., Young R.P., Oates S.J. 2002. Numerical modeling of seismicity induced by fluid injection in a fractured reservoir. In: Mining and Tunnel Innovation and Opportunity, In: Proceedings of the 5th North American Rock Mechanics Symposium, Toronto, Canada, pp. 1023-1030.

12. Hillis R. 2000. Pore pressure/stress coupling and its implications for seismicity. Exploration Geophysics 31, 448-454.

13. Hökmark H., Lönnqvist M., Fälth B. 2010. THM-issues in repository rock-Thermal, mechanical, thermo-mechanical and hydro-mechanical evolution of the rock at the Forsmark and Laxemar sites. SKB-Swedish Nuclear Fuel and Waste Management Co. Technical Report TR-10-23.

14. Itasca Consulting Group Inc. 2008. PFC2D-Particle Flow Code in 2 Dimensions, Version 4.0. Minneapolis.

15. Kohl T., Megel T. 2007. Predictive modeling of reservoir response to hydraulic stimulations at the European EGS site Soultz-sous-Forets. International Journal of Rock Mechanics and Mining Sciences 44(8), 1118-1131.

16. Kraft T., Mai P.M., Wiemer S., Deichmann N., Ripperger J., Kästli P., Bachmann C., Fäh D., Wössner J., Giardini D. 2009. Enhanced Geothermal Systems: Mitigating Risk in Urban Areas. EOS 90(32), 11 August 2009.

17. Kramer S.L. 1996. Geotechnical Earthquake Engineering, Prentice-Hall, Englewood Cliffs, N.J. 653.

18. Majer E.L., Baria R., Stark M., Oates S., Bommer J., Smith B., Asanuma H. 2007. Induced seismicity associated with Enhanced Geothermal Systems. Geothermics 36, 185-222.

19. McClure M., Horne R. 2011. Investigation of injection-induced seismicity using a coupled fluid flow and rate and state friction model. Geophysics 76(6), WC183-WC200.

20. Mukuhira Y., Asanuma H., Niitsuma H., Häring M.O. 2013. Characteristics of large-magnitude microseismic events recorded during and after stimulation of a geothermal reservoir at Basel, Switzerland. Geothermics 45, 1-17.

21. Potyondy D.O., Cundall P.A. 2004. A bonded-particle model for rock. International Journal of Rock Mechanics Mining Sciences 41, 1329-1364.

22. Rutqvist J., Birkholzer J., Cappa F., Tsang C.-F. 2007. Estimating maximum sustainable injection pressure during geological sequestration of CO_2 using coupled fluid flow and geomechanical fault-slip analysis. Energy Conversion and Management 48,1798-1807.

23. Schoenball M., Müller T.M., Müller B., Heidbach O. 2010. Fluid-induced microseismicity in pre-stressed rock masses. Geophysical Journal International 180, 113-119.

24. Yoon J.S., Zang A., Stephansson O. 2012. Simulating fracture and friction of Aue granite under confined asymmetric compressive test using clumped particle model. International Journal of Rock Mechanics Mining Sciences 49, 68-83.

25. Yoon J.S., Zang A., Stephansson O. 2013. Simulation of hydraulic stimulation of fractured reservoir and induced seismicity using discrete element-fracture network model. In: Proceedings of Thirty-Eighth Workshop on Geothermal Reservoir Engineering, Stanford University, Stanford, California, February 11-13, 2013, SGP-TR-198.

26. Zang A., Stephansson O. 2010. Stress Field of the Earth's Crust. Springer Science + Business Media B.V., Dordrecht.

27. Zang A., Yoon J.S., Stephansson O., Heidbach O. 2013. Fatigue hydraulic fracturing by cyclic reservoir treatment enhances permeability and reduced induced seismicity. Geophysical Journal International 195, 1282-1287.

28. Zhao X., Young R.P. 2011. Numerical modelling of seismicity induced by fluid injection in naturally fractured reservoirs. Geophysics 76(6), WC167-WC180.

Yoon, Jeoung Seok

2000 Handong Global University, Korea, B.Sc.in Construction, Urban and Environmental Engineering
(2002년 한동대학교 건설도시환경공학부 공학사)
2002 Seoul National University, Korea, M.Sc. in Civil, Urban and Geosystem Engineering
(2002년 서울대학교 지구환경시스템공학부 공학석사)
2007 Seoul National University, Korea, Ph.D. in Civil, Urban and Geosystem Engineering
(2007년 서울대학교 지구환경시스템공학부 공학박사)
Tel: +49-331-288-1716
E-mail: jsyoon@gfz-potsdam.de
Current affiliation: Helmholtz Centre Potsdam, GFZ German Research Centre for Geosciences, Section 2.6 Seismic Hazard and Stress Field

Zang, Arno

1987 Johann Wolfgang Goethe-University Frankfurt/Main, Germany, Diploma Geophysics
1991 Johann Wolfgang Goethe-University Frankfurt/Main, German, Ph.D. Geophysics
1998 University of Potsdam, Germany, Habilitation Geophysics
Tel: +49-331-288-1325
E-mail: arno.zang@gfz-potsdam.de
Current affiliation: Helmholtz Centre Potsdam, GFZ German Research Centre for Geosciences, Section 2.6 Seismic Hazard and Stress Field

Hakimhashemi, Amir

1996 Isfahan University of Technology, Iran, B.Sc. in Applied Mathematics
1999 Institute for Research in Planning and Development, Iran, M.Sc. in Socioeconomic System Engineering
2006 Kaiserslautern University of Technology, Iran, M.Sc. in Mathematics, Optimization and Statistics
2010 University of Potsdam, Germany, Ph.D. in Applied Geophysics
Tel: +49-331-288-1264
E-mail: amir.hakimhashemi@gfz-potsdam.de
Current affiliation: Helmholtz Centre Potsdam, GFZ German Research Centre for Geosciences, Section 2.6 Seismic Hazard and Stress Field

Zimmermann, Günter

1987 Bonn University, Germany, Diploma Physics
1991 Technical University Berlin, Germany, Ph.D. Applied Geophysics
2006 Technical University Berlin, Germany, Habilitation Applied Geophysics
2012 Technical University Berlin, Germany, Professor Applied Geophysics
Tel: +49-331-288-1458
E-mail: guenter.zimmermann@gfz-potsdam.de
Current affiliation: Helmholtz Centre Potsdam, GFZ German Research Centre for Geosciences, Section 4.1 Reservoir Technologies & International Centre for Geothermal Research (ICGR)